University of Szeged
Doctoral School of Computer Science

Image Analysis Methods for Biomedical and Industrial Applications

Summary of the Doctoral Theses

Melinda Katona

Supervisor:

László G. Nyúl, PhD

Szeged
2019

1 Introduction

Imaging technology is at an advanced level of development nowadays and the processing of large amounts of image data raises many image processing and image analysis problems. In this dissertation, we address the various problems of image analysis in areas of medical image based diagnostics, microscopy in biology, and localization of visual codes. In cases when the structure of the object is well defined it can be expected that an image analysis method provides acceptable results automatically, such as for processing visual codes. In other cases, e.g., the interpretation of medical images can be uncertain even for human experts, thus here we aim to give only assistance that the doctors can use in diagnosis. Classical image processing approaches are well applicable for various detection and segmentation tasks and these do not require a large set of image data which was not available during our work. Besides, in recent years deep neural networks became widespread in image processing. These try to provide more general solutions in many areas. Their disadvantage is that the methods require a large amount of data for training. The methods presented in the dissertation are based on classical image processing operations, but we also applied a deep learning approach to one of the retina analysis tasks.

The dissertation consist of three main parts: analysis of retinal images in Chapter 2, detection of morphological changes in zebrafish embryos in Chapter 3, and localization of visual codes in Chapter 4.

2 Retinal Image Analysis

The human eye is the sense organ of vision in the human body that reacts to the rays of light emanating from environmental objects and maps their shape, spatial position and color. Incoming rays of light pass through the vitreous and focus on the retina. The retina is the sensory membrane and composed of several layers, including photoreceptors which take light focused by the cornea and lens. The small central area of the retina called the macula. This region of the retina is responsible for central vision. Different diseases that can affect the eye. Several imaging techniques are available to investigate the retina. A modern tool for *age-related macular degeneration* (AMD) examination is *optical coherence tomography* (OCT). AMD is a common eye condition among people above 50 years worldwide, currently affecting 170 million people globally. Existing OCT systems show many features about AMD, such as measurable indicators of some biological state or condition that so-called as OCT biomarkers. To improve the treatment procedure, there is a need for more precise measurements, hence our aim was to create automatic methods for quantitative assessment of biomarkers (see in Figure 1).

2.1 Delineation of boundary layers

The location and thickness measurement of retinal layers provides useful information for detecting pathological changes and diagnosing different type of retinal diseases. We proposed two approaches to delineate *internal limiting membrane* (ILM) and retinal pigment epithelial (RPE) boundary layers. The quality of the OCT images are usually low, so often requires pre-processing to improve contrast and normalize intensity levels thus we use

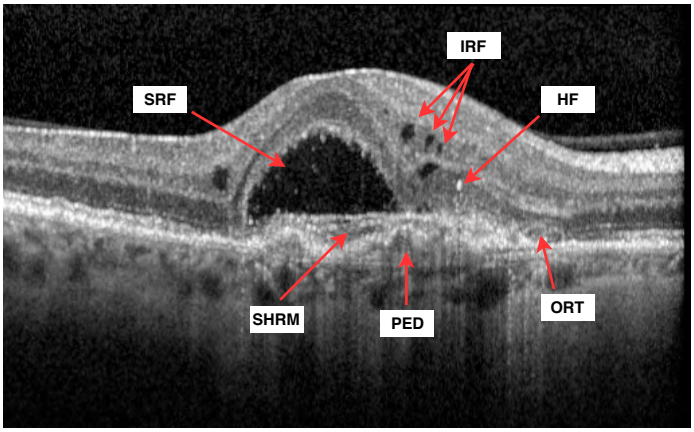

Figure 1: Various types of biomarkers of AMD. Subretinal fluid (SRF), intraretinal fluid (IRF), hyperreflective foci (HF), subretinal hyperreflective material (SHRM), pigment epithelial detachment (PED), outer retinal tubulation (ORT).

noise filtering and contrast enhancement using a fuzzy operator [1]. The vertical profiles of the filtered image are noisy thus we use Savitzky-Golay smoothing filter which is effective at preserving the pertinent high frequency components of the signal. Figure 2 presents an example. For each filtered vertical profiles, the large intensity steps in pixel density are assumed to correspond to change of tissue.

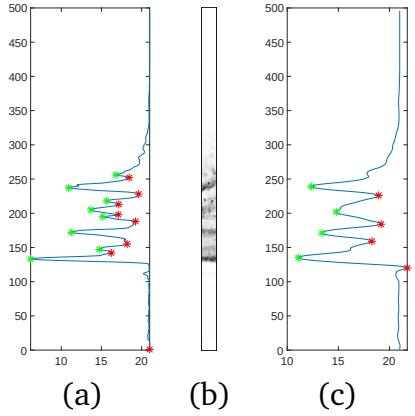

Figure 2: Calculated horizontal projection for vertical profile analysis. (a) original data, (b) sample bar, (c) Savitzky-Golay filtered data (polynomial order: 3, frame length: 25)

This approach showed many inadequate results in RPE layer detection when AMD causes highly distorted layers hence we developed a new approach. Graph cut is used to optimize k-means partitioning. The ILM elevation can be determined after a simple Otsu thresholding because the foreground and background can be clearly distinguished from that part of the retina in the clustered image. Similarity to the previous method, we calculate vertical projection in every 10th column to determine boundary and we choose the local minimum from the projected data.

2.2 Measurement of retina distortion

The dysfunction of RPE cells contributes to a series of pathological processes and this layer can locally detach from the underlying Bruch's membrane and fluid can accumulate underneath the RPE and/or within the retina. In addition to the unambiguously specified biomarkers in the case of AMD, the measure and start and end points of distorted regions are also a useful descriptor for medical doctors in diagnosis.

From the defined ILM layer points we select the smallest y coordinate and the image splitted into two parts using this point. We also determine the highest y coordinates from the ILM points in the right and left retinal segment to define starting and end point of the distortion. A line is fitted to the assigned minimal y point and we investigate the distance of the ILM layer points and the line. If the distance is smaller than a threshold value, the layer is not distorted. Figure 3 summarizes our approach that use previously defined ILM layer points. Additionally, it is feasible to determine the possible normal layer boundary if we delineate the RPE layer earlier.

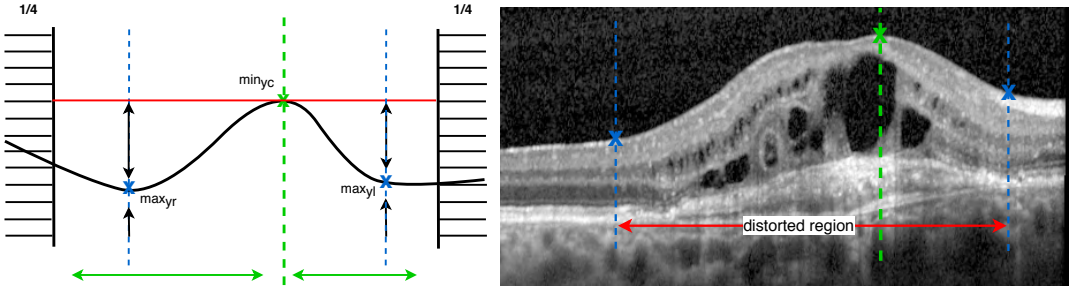

Figure 3: Schematic view of the determination of distortion. min_{yc} denotes the smallest y coordinate from ILM points. A line is fitted to this point (Red line). max_{yr} and max_{yl} are the highest y coordinates in the right and left retinal segments.

2.3 Detection of subretinal and intraretinal fluid

It can be observed that subretinal fluid regions appear as spots with brighter intensity in the image. The zones of the disease and the intensity of the vitreous body of the eye are almost within the same range if distortions are not considered. Observations showed that SRF regions are close to the RPE layer and near/in the distorted area. We investigate the vertical stripes, and based on the above assumptions, we look for minimum locations on the horizontal projections that are closest (and the second one closest) to the RPE layer. We consider only the profile between ILM and RPE points. Using the average layer thickness and vessel shadow information, we can filter out the stripes which are less reliable than the others approximating the fluid segments.

The reflectivity of the IRF biomarker is similar to the SRF and appears as smaller oval object that are located near RPE layer. Based on this a priori information, we have developed a method that can simultaneously segment and differentiate fluid areas using edge-based active contour process. This method use mask that is created in previous steps of our approach. To seperate the biomarkers, we used a condition set based on shape characteristic and the position of the object. We re-implemented two existing methods according to the original papers for comparison [19, 20].

Automatically calculated quantitative descriptors can be visually presented to the medical doctor to aid interpretation of data. The first type of visualization is the traditional slice-by-slice display which provides a good depth context within slice, but no spatial context between slices. Figure 4 represents restricted subretinal fluid area which results were verified by ophthalmologists and they found the segmentation, quantification and also the visualization technique useful.

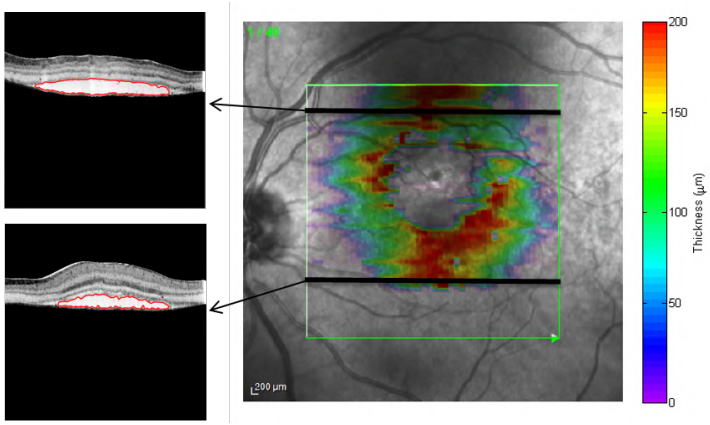

Figure 4: Color overlay of the subretinal fluid volume thickness. Left: Red boundaries indicate the subretinal fluid in each slice. Right: The color/hue relates to subretinal fluid thickness.

2.4 Determination of pigmentepithel detachment and subretinal hyperreflective material

Automatic detection of abnormal retinal structures remains a challenging task. The retinal morphology and intensity may change acutely resulting from the abnormal structures and the prior knowledge about morphological and optical features clues that are used for normal retinal image segmentation may not be valid. Subretinal Hyperreflective Material, as its name suggests, is likely composed of many components, including fluid, fibrin, blood, etc., and its composition changes over time. So, the reflectivity of SHRM is heterogeneous. In contrast, Pigment Epithelial Detachment has lower intensity, so these can be separated from each other. Nevertheless, in many cases, due to the above introduced reasons, their location and presence are unclear. In some cases, abnormalities are so inseparable that they are managed as one.

Our method is based on the introduced graph cut approach, but the definition of specific segments is determined by different conditions. The location of the possible SHRM has played an important role in determining PED. In many cases, SHRM is not clearly detectable as can be seen in Figure 5.

2.5 Segmentation of outer retinal tubulation

Outer retinal tubulation (ORT) was first described by Zweifel et al. [22] as “hyporeflective tubular structures with hyperreflective borders within the nuclear layer of the retina” and appear in many retinal diseases.

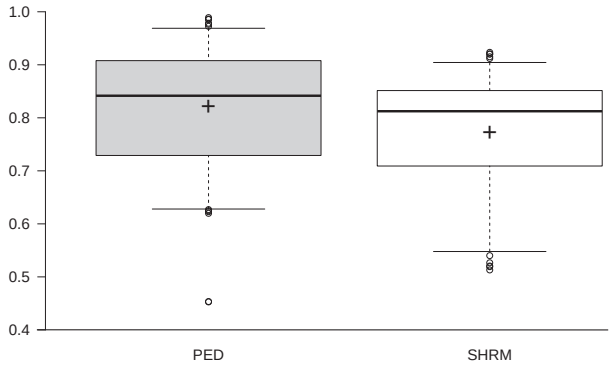

Figure 5: Box plots representing the Dice coefficients of PED and SHRM generated by our method. In both cases, the mean Dice coefficients were greater than 0.7. Black cross = mean Dice coefficient; empty circles = outliers; PED = pigment epithelial detachment; SHRM = subretinal hyperreflective material.

We proposed a method using simple image processing operations to detect ORT. This method based on finding hyperreflective points. In this case to reduce noise, Wiener filter is applied. Reflective points are localized using a Hessian detector. For filtering out the false points, we use some prior information about the biomarkers such as subretinal and intraretinal fluid, retinal thickness, etc. Limiting the specific extent of the ORT in many cases is very difficult, because there is no clear distinction between the hyperreflective wall and its surroundings. Since we assume that ORT contains hyperreflective points, we compute distance map, threshold it and finally the convex hull of the objects is determined.

The classical operation based method is not robust against more diverse images thus we have developed a more general approach, so we consider a sligthly modified version of the original U-Net architecture for detecting ORT. There are three differences:

- we reduce the number of layers to speed up training time,
- we double the number of filters in each layer to give larger capacity to the model, since the amount of data augmentation and retorsion in the orignal images are high, hence we expect the model to be invariant to this transformation,
- to prevent overfitting, we use Dropout between every convolutional layers except the last two ones.

The available amount of training data is extremely small, 132 examples, but machine learning techniques profit from more training data and more data can help reduce overfitting thus we use real time augmentation technique during training. Since our dataset contains sequences from only nine patients, we use nested cross-validation for hyperparameter tuning and measuring the test error. The input is the whole OCT image and stochastic gradient descent (SGD) is used for optimizing the loss function with one sample per update.

Dice coefficient measures well how precise a segmentation, is however our main goal is not a perfect segmentation of ORT, only the cardinality of the objects. To fulfill this goal, in addition to the Dice coefficient we measured the recall of the ORT objects. Table 1 shows the achieved Dice and Recall values on K-fold validation, the rows are the results of the

medical doctors against each other the annotator, in case of MD_1 against MD_2 and our modified U-Net architecture against the union of the masks of MD_1 and MD_2.

Table 1: Object level based and global performance of the doctors and trained models.

	Recall (object)	Dice (global)	Dice (object)
MD_1	0.908	0.682	0.665
MD_2	0.812	0.625	0.590
U-Net	0.847	0.579	0.583

3 Quantitative Analyis of Irradiated Zebrafish Embyros

Research is ongoing in many areas of life and one of the most important is how to treat cancer more effectively. Radiotherapy is one of the most common methods to treat different cancer cells in clinical application despite having harmful effects on healthy tissues. Radiobiological experiments are very important to determine the irradiation-caused acute and chronic effects to define the exact consequences of different irradiation sources. Photon irradiation has been used on zebrafish embryos a very new *in vivo* and appropriate model system in radiobiology. After irradiation, dose-dependent morphological changes were observable in the embryos. The advantage of using zebrafish vertebrate model is the biological changes assessment on large number of embryos, enabling high power statistical analysis. The evaluating process for one study can contain take several weeks for the biologists to complete, we introduce a framework to reduce human effort for faster experimentation.

There are many methods in the literature for analyzing microscopic images of zebrafish embryos, but these only provide a solution to one of a sub-problem. Before analysis of the morphological changes, sorting and improve quality of images are needed that may be blurred, the well does not contain fish or the embryo perished. The sides of the well also appears in images, we proposed an approach to detect. The various shape characteristics of zebrafish is obtained in order to give a quicker picture of the response of fish to irradiation. A procedure is presented that is capable of delimiting the area of the zebrafish, localizing the eye or the eyes, determining their diameter, the distance between the head and tail of the fish, and giving the position of the fish. The results are compared and contrasted with manually annotated data by biologists. Figure 6 illustrates segmentation results by the algorithm for some cases.

4 Localization of Visual Codes

Visual codes play an important role in automatic identification, which became an inseparable part of industrial processes. Thanks to the revolution of smartphones and telecommunication, it also becomes more and more popular in everyday life, containing embedded web addresses or other small informative texts.

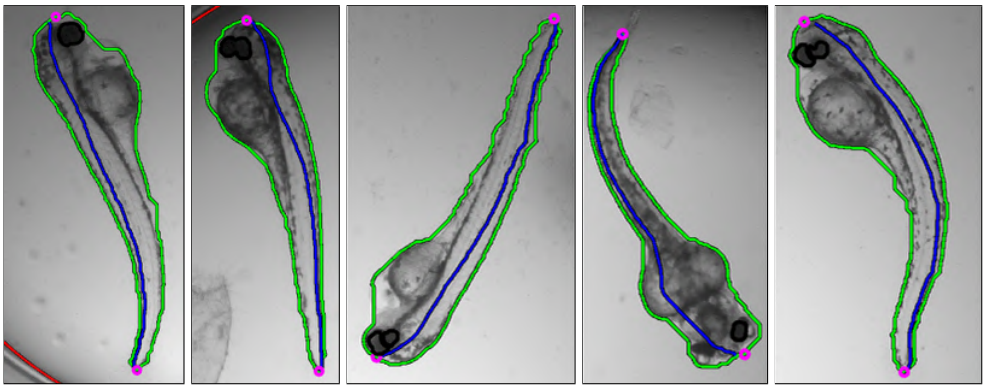

Figure 6: Illustration of detected zebrafish embryos with their eye/eyes and end points.

While barcode reading is straightforward in images having optimal parameters (focus, illumination, code orientation, and position), localization of code regions is still challenging in many scenarios. Every setup has its own characteristics, therefore many approaches are justifiable. Industrial applications are likely to have more fixed parameters like illumination, camera type and code size, and processing speed and accuracy are the most important requirements. In everyday use, like with smartphone cameras, a wide variety of code types, sizes, noise levels and blurring can be observed, but the processing speed is often not crucial, and the image acquisition process can be repeated in order for successful detection.

4.1 Mathematical morphology based algorithms

Mathematical morphology is useful for the analysis and processing of geometrical structures in images. Our algorithm based on bottom-hat filtering and consists of two main phases. The input image is converted to grayscale in the preprocessing phase, because although barcodes may be printed in various colors, the pattern of dark bars on a light background is equivalent. To reduce the image noise, we used Gaussian smoothing and bottom-hat filtering to highlight edges in image. In order to detect possible barcode regions, the edge-enhanced image is binarized with global thresholding for finding possible barcode segments, but so far may contain false regions. These false regions are eliminated using an area threshold. Since a barcode consists of a sequence of parallel bars and the bars are located at varying distance from each other, they do not compose a connected component. Therefore in this phase we use dilation to merge these patterns.

In order to improve the method introduced, we use another aspect to localize barcode regions after binarization since we observed worse results under poor lighting. Also we take the advantage of the structure of the barcode, the fact that it consists of approximately regularly spaced parallel stripes. Here, for each pixel, we calculate the Euclidean distance of the pixel from the nearest nonzero pixel. Using the distance map, objects that are far from other objects can be easily dropped, and only nearby objects (sort of a cluster of bar segments) will be kept. To remove unwanted objects, we used the same steps as in the original procedure, but with different structure elements and thresholds. We summarize the intermidiate key stages of the algorithms in Figure 7.

We compared the effectiveness of the proposed methods with some approaches from

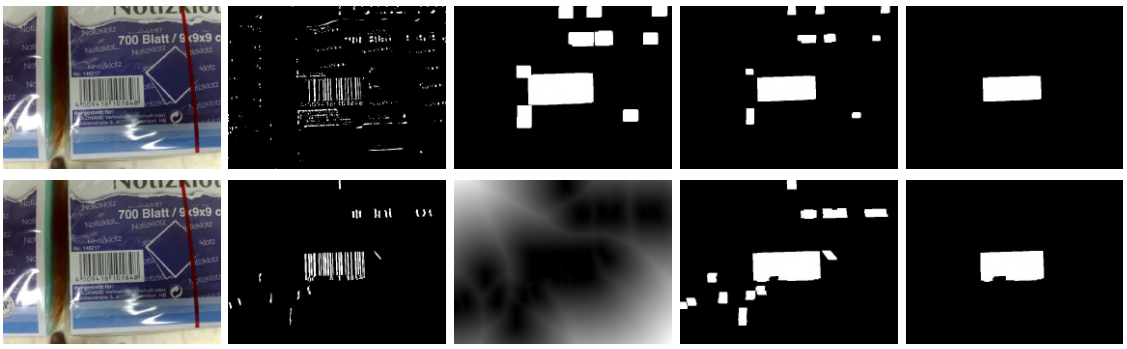

Figure 7: Intermediate steps of the algorithm based on bottom-hat transform (top row) and its improved approach to localize 1D traditional barcodes (bottom row) at key phases.

the literature [3, 8, 18]. Our proposed algorithms are very fast. In most cases, faster procedures locate barcodes less accurately or not at all, as if loss of accuracy were the price for the speed gain. However, in our case, speed is not coupled with a significant cost in accuracy.

4.2 Detection using template matching

Pattern matching is an approach to find the location of a template image. Since classical 1D barcodes show similar patterns and 2D codes we can also observe specific features, thus pattern matching may be a possible solution for detection.

We proposed a method to detect 1D barcodes using template matching. Similarly to previously described methods, the quality of the image is improved in preprocessing phase. The detection process is based on binary images, so the image is binarized using a global threshold. This is not a robust solution, but selecting valid regions from false regions is easier than finding a missing part during a post-processing process. The shape of the bars of a barcode are rectangular, so we examine the shape of each object formed by connected binary components. If the shape of the object is not approximately rectangular, we do not consider it as a candidate region. The input template for pattern matching consists of two parallel lines. The process of template matching occurs in the frequency domain using Fast Fourier Transformation. The set of points from template matching are well-separable like the bars of the barcode that are close to each other. To keep valid regions, we use a priori information about the barcode. In order to determine the whole barcode region, we use morphological opening with a square-shaped structuring element. The size is defined based on the maximal distance between the stripes, which provides that every barcode will have its own connected region. This method also works on stacked 2D barcodes.

Based on another template, the method can be adapted with modifications to determine the location of QR codes. In order to highlight the barcode areas, we use standard deviation based adaptive filtering method. The resulting image is heterogeneous, so we calculate the number of object points for every kernel and remove the actual segment from possible barcode regions. Based on empirical observations, we binarize the image obtained in the previous step and we can eliminate numerous false segments. Code segments are validated using pattern matching. For this, we used a small QR code as a sample.

Our approaches were compared against other algorithms in the literature using the

Muenster database in the case of 1D codes and Dubská for QR as a benchmark [2, 4, 6, 7, 21].

Some qualitative results the approaches are presented on challenging images that are illuminated, geometry distorted and contains several objects similar to a barcode in Figure 8.

Figure 8: Qualitative results of the proposed methods on some challenging 1D and QR images.

4.3 Validating authenticity of visual codes in an industrial application

Codes are designed using commonly used geometric patterns usually identify types or individuals. However, patterns that are unique in nature and can therefore be used to verify originality or authenticity can be produced. The identifying label in this case contains a combination of artificial and natural feature identifiers. A standard QR code of a given size is in the center of the label area. This code can encode any content relevant in the application context, e.g. a serial number or a key into a database. Figure 9 shows a schematic drawing of the label layout and an image of a real piece of a prototype label.

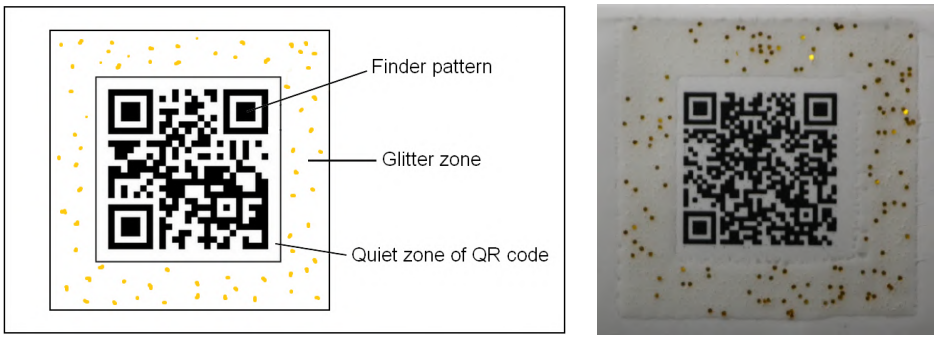

Figure 9: A sketch of the NFI label layout (left) and an image of a real prototype label (right).

Depending on the label specification, different image processing approaches are required. Thus, our image processing pipeline consists of the following major steps:

1. locate the QR code (position and orientation),
2. delineate the glitter zone,
3. find the glitters,
4. extract features from the glitter pattern.

We outline the process of identification or NFI recognition that can be performed using features extracted in the previous image processing phase. Each of the following subtasks can be solved in various simple or more sophisticated ways:

1. find matching points,
2. calculate similarity measure,
3. decide about acceptance or rejection.

In our prototype implementation we used image-based features for validation, solely the normalized position of the centroid of the detected glitter. At this stage of the deveplopment this was enough for an appropriate validation. Regardless of the simplicity of this setup, the results reported below show the feasibility of such NFI technology using mobile applications.

5 Contributions of the thesis

Contributions in the first group are related to the investigation of various biomarkers of age-related macular degeneration on Optical Coherence Tomography (OCT) images.

I/1. I proposed two new approaches to define inner limiting membrane (ILM) and retinal pigment epithelial (RPE).

I/2. I developed a new method to determine the position and extent of the distortion which is an important feature in the prognosis of AMD.

I/3. I proposed two new algorithms to detect subretinal fluid (SRF) and cysts.

I/4. I developed an approach to determine pigment epithelial detachment (PED) and subretinal hyperreflective material (SHRM).

I/5. I proposed a new method based on classical operations and I suggested a convolutional neural network to localize outer retinal tubulation (ORT).

Contributions in the second thesis point are related to automatic detection of morphological deteriorations of irradiated zebrafish embryos in microscopic images used in radiobiological research.

II. I developed a new algorithm to delineate the zone of the well and to obtain various morphological features of zebrafish: the endpoints and length of the embryos, the position and diameter of the eye or eyes, the orientation of the fish. I compared the results with manually annotated data by biologists.

Contributions in the third group are related to localization of visual codes in digital images.

III/1. I proposed two new methods based on morphological operations to localize traditional 1D and stacked 2D barcodes.

III/2. I developed a new approach to detect classical 1D barcodes and another one to segment QR codes using pattern matching.

III/3. I proposed a method to localize and recognize a hybrid visual code (NFI).

III/4. I performed an extensive comparative analysis of 12 code localization methods on publicly available and on our own databases of tens of thousands of real and synthetic images depicting 1D and 2D codes.

Table 2 summarizes the relation between the thesis points and the corresponding publications.

Table 2: Correspondence between the thesis points and the publications.

Publication	Thesis point									
	1.1	1.2	1.3	1.4	1.5	2	3.1	3.2	3.3	3.4
[12]	•	•	•							
[14]			•							
[15]					•					
[17]	•			•						
[5]					•					
[16]						•				
[9]							•			•
[10]							•			•
[11]									•	
[13]								•		•

References

[1] J. Dombi. *Modalities*, pages 53–65. Springer Berlin Heidelberg, 2012.

[2] O. Gallo and R. Manduchi. Reading 1D Barcodes with Mobile Phones Using Deformable Templates. *IEEE Trans. Pattern Anal. Mach. Intell.*, 33(9):1834–1843, 2011.

[3] J. Juett and X. Qi. Barcode localization using bottom-hat filter. *NSF Research Experience for Undergraduates*, 2005.

[4] D-T. Lin and C-L. Lin. Automatic location for multi-symbology and multiple 1d and 2d barcodes. *Journal of Marine Science and Technology*, 21:663–668, 2013.

[5] I. Megyeri, M. Katona, and L. G. Nyúl. A Novel Approach to Detect Outer Retinal Tubulation using U-net in SD-OCT images. Submitted. 2019.

[6] E. Ohbuchi, H. Hanaizumi, and L. A. Hock. Barcode Readers Using the Camera Device in Mobile Phones. In *Proceedings of the 2004 International Conference on Cyberworlds*, CW '04, pages 260–265, 2004.

[7] G. Sörös and C. Flörkemeier. Blur-resistant Joint 1D and 2D Barcode Localization for Smartphones. In *Proceedings of the 12th International Conference on Mobile and Ubiquitous Multimedia*, pages 11:1–11:8, 2013.

[8] E. Tekin and J. M. Coughlan. An algorithm enabling blind users to find and read barcodes. In *Applications of Computer Vision (WACV), 2009 Workshop on*, pages 1–8, 2009.

[9] M. Katona and L. G. Nyúl. A Novel Method for Accurate and Efficient Barcode Detection with Morphological Operations. In *2012 Eighth International Conference on Signal Image Technology and Internet Based Systems*, pages 307–314, 2012.

[10] M. Katona and L. G. Nyúl. Efficient 1D and 2D Barcode Detection Using Mathematical Morphology. In *Mathematical Morphology and Its Applications to Signal and Image Processing*, pages 464–475. Springer Berlin Heidelberg, 2013.

[11] M. Katona and L. G. Nyúl. Fast Recognition of Natural Feature Identifiers by a Mobile Phone. *Acta Cybernetica*, 22:101–116, 2015.

[12] M. Katona and L. G. Nyúl. An Approach to the Quantitative Assessment of Retinal Layer Distortions and Subretinal Fluid in SD-OCT Images. *Acta Cybernetica*, 23:615–628, 2017.

[13] M. Katona, P. Bodnár, and L. G. Nyúl. Distance Transform and Template Matching Based Methods for Localization of Barcodes and QR Codes. *Computer Science and Information Systems*. doi: https://doi.org/10.2298/CSIS181011020K.

[14] M. Katona, A. Kovács, R. Dégi, and L. G. Nyúl. Automatic Detection of Subretinal Fluid and Cyst in Retinal Images. In *Image Analysis and Processing – ICIAP 2017*, pages 606–616, 2017.

[15] M. Katona, A. Kovács, L. Varga, T. Grósz, J. Dombi, R. Dégi, and L. G. Nyúl. Automatic detection and characterization of biomarkers in oct images. In Aurélio Campilho, Fakhri Karray, and Bart ter Haar Romeny, editors, *Image Analysis and Recognition – ICIAR 2018*, pages 706–714, Cham, 2018. Springer International Publishing. doi: 10.1007/978-3-319-93000-8_80.

[16] M. Katona, T. Tőkés, E. R. Szabó, Sz. Brunner, I. Z. Szabó, R. Polanek, K. Hideghéty, and L. G. Nyúl. Automatic Segmentation and Quantitative Analysis of Irradiated Zebrafish Embryos. In *Computational Modeling of Objects Presented in Images. Fundamentals, Methods, and Applications*, pages 95–107, 2019.

[17] M. Katona, A. Kovács, R. Dégi, and L. G. Nyúl. Segmentation of Subretinal Hyperreflective Material and Pigment Epithelial Detachment Using Kernel Graph Cut. In *Progress in Computer Recognition Systems*, pages 98–105. Springer International Publishing, 2020.

[18] T. R. Tuinstra. *Reading Barcodes from Digital Imagery*. PhD thesis, Cedarville University, 2006.

[19] W. Wieclawek. Automatic cysts detection in optical coherence tomography images. In *Mixed Design of Integrated Circuits Systems (MIXDES), 2015 22nd International Conference*, pages 79–82, 2015.

[20] G. R. Wilkins, O. M. Houghton, and A. L. Oldenburg. Automated Segmentation of Intraretinal Cystoid Fluid in Optical Coherence Tomography. *IEEE Transactions on Biomedical Engineering*, 59(4):1109–1114, 2012.

[21] I. Yun and J. Kim. Vision-based 1D barcode localization method for scale and rotation invariant. In *TENCON 2017 - 2017 IEEE Region 10 Conference*, pages 2204–2208, 2017.

[22] S. A. Zweifel, M. Engelbert, K. Laud, R. Margolis, R. F. Spaide, and K. B. Freund. Outer Retinal Tubulation: A Novel Optical Coherence Tomography Finding. *JAMA Ophthalmology*, 127(12):1596–1602, 2009.

The author's publications on the subjects of the thesis

Journal publications

M. Katona and L. G. Nyúl. Fast Recognition of Natural Feature Identifiers by a Mobile Phone. *Acta Cybernetica*, 22:101–116, 2015.

M. Katona and L. G. Nyúl. An Approach to the Quantitative Assessment of Retinal Layer Distortions and Subretinal Fluid in SD-OCT Images. *Acta Cybernetica*, 23:615–628, 2017.

M. Katona, P. Bodnár, and L. G. Nyúl. Distance Transform and Template Matching Based Methods for Localization of Barcodes and QR Codes. *Computer Science and Information Systems*. doi: https://doi.org/10.2298/CSIS181011020K.

Full papers in conference proceedings

M. Katona and L. G. Nyúl. A Novel Method for Accurate and Efficient Barcode Detection with Morphological Operations. In *2012 Eighth International Conference on Signal Image Technology and Internet Based Systems*, pages 307–314, 2012.

M. Katona and L. G. Nyúl. Efficient 1D and 2D Barcode Detection Using Mathematical Morphology. In *Mathematical Morphology and Its Applications to Signal and Image Processing*, pages 464–475. Springer Berlin Heidelberg, 2013.

M. Katona, A. Kovács, R. Dégi, and L. G. Nyúl. Automatic Detection of Subretinal Fluid and Cyst in Retinal Images. In *Image Analysis and Processing – ICIAP 2017*, pages 606–616, 2017.

M. Katona, A. Kovács, L. Varga, T. Grósz, J. Dombi, R. Dégi, and L. G. Nyúl. Automatic detection and characterization of biomarkers in oct images. In Aurélio Campilho, Fakhri Karray, and Bart ter Haar Romeny, editors, *Image Analysis and Recognition – ICIAR 2018*, pages 706–714, Cham, 2018. Springer International Publishing. doi: 10.1007/978-3-319-93000-8_80.

M. Katona, A. Kovács, R. Dégi, and L. G. Nyúl. Segmentation of Subretinal Hyperreflective Material and Pigment Epithelial Detachment Using Kernel Graph Cut. In *Progress in Computer Recognition Systems*, pages 98–105. Springer International Publishing, 2020.

M. Katona, T. Tőkés, E. R. Szabó, Sz. Brunner, I. Z. Szabó, R. Polanek, K. Hideghéty, and L. G. Nyúl. Automatic Segmentation and Quantitative Analysis of Irradiated Zebrafish Embryos. In *Computational Modeling of Objects Presented in Images. Fundamentals, Methods, and Applications*, pages 95–107, 2019.

I. Megyeri, **M. Katona**, and L. G. Nyúl. A Novel Approach to Detect Outer Retinal Tubulation using U-net in SD-OCT images. In *The 15th International Conference on Signal Image Technology & Internet Based Systems*, 2019. Submitted for publication.

Further related publications

M. Katona and L. G. Nyúl. Improved 1D and 2D barcode detection with morphological operations. In *A Képfeldolgozók és Alakfelismerők Társaságának 9. országos konferenciája - KÉPAF 2013*, pages 309–324, 2013.

M. Katona and L. G. Nyúl. Fast recognition of natural feature identifiers by a mobile phone. In *The 9th Conference of PhD Students in Computer Science (CSCS 2014) : Volume of Extended Abstracts*, page 26, 2014.

Katona M. and Nyúl L. G. Vonalkódok és természetes vizuális azonosítók felismerése valós időben. In *A Képfeldolgozók és Alakfelismerők Társaságának 10. országos konferenciája - KÉPAF 2015*, pages 562–577, 2015.

R. Dégi, A. Kovács, **M. Katona** , L. G. Nyúl, L. G. Varga, J. Dombi, and T. Grósz. Quantitative assessment of the manifestation of age-related macular degeneration via automated image analysis of spectral-domain optical coherence tomography. In *European Society of Retina Specialists 15th EURETINA Congress*, page 1 p., 2015.

Varga L., **Katona M.**, Grósz T., Dombi J., Kovács A., Dégi R., and Nyúl L. G. Időskori makula degeneráció kvantitatív jellemzése SD-OCT képek automatikus elemzésével. In *Új alapokon az egészségügyi informatika : A XXVIII. Neumann Kollokvium konferenciakiadványa*, pages 43–48, 2015.

M. Katona and L. G. Nyúl. Quantitative Assessment of Retinal Layer Distortions and Subretinal Fluid in SD-OCT Images. In *The 10th Conference of PhD Students in Computer Science (CSCS 2016) : Volume of Extended Abstracts*, page 37, 2016.

A. Kovács, R. Dégi, **M. Katona**, L. G. Nyúl, L. Varga, J. Dombi, and T. Grósz. Biomarkerek automatikus karakterizálása OCT felvételek időbeli elemzésére. In *Magyar Szemorvostársaság Retina Szekciójának Kongresszusa*, page 1 p., 2017.

Katona M., Tőkés T., Szabó E. R., Brunner Sz., Polanek R., Hideghéty K., and Nyúl L. G. Sugárkezelésen átesett zebrahal embriók automatikus morfológiai elemzése. In *A Képfeldolgozók és Alakfelismerők Társaságának 12. országos konferenciája - KÉPAF 2019*, page Paper 21. 12 p., 2019.